Energy rectification in active gyroscopic networks under time-periodic modulations

Zhenghan Liao [1,*] and Suriyanarayanan Vaikuntanathan[1,2,†]

[1]*Department of Chemistry, University of Chicago, Chicago, Illinois 60637, USA*
[2]*James Franck Institute, University of Chicago, Chicago, Illinois 60637, USA*

Combinations of gyroscopic forces and nonequilibrium activity have been explored recently in rectifying energy in networks with complex geometries and topologies [Phys. Rev. X **10**, 021036 (2020)]. Based on this previous work, here we study the effect of added time-periodic modulations. Numerical calculations show that the time-modulated network generates net energy transport between sites and the surroundings, even in the absence of any temperature gradients. Combining path integral formulation and diagrammatic expansion, we explain how such anomalous energy transport emerges, and show how the transport pattern in complex networks can be connected to relatively simple local structures.

I. INTRODUCTION

Pioneering studies on energy rectification have shown how energy fluxes can be generated in the absence of temperature biases [1–13]. Such principles can potentially be applied to build nanoscale energetic rectifiers [6]. From a theoretical perspective, energy transport is usually associated with phonons, but these collective excitations are more difficult to manipulate compared with single particles [6,14]. Previous studies have exploited opportunities provided by nonlinear interactions [4], athermal baths [2], geometric phases from adiabatic modulations [5], or quantum Floquet systems [15]. Using a combination of parity-breaking metamaterials and nonequilibrium forcing, our recent work [16] uncovered new rectification principles which manifest as directed energy flows between sites in network systems. Unlike many previous studies that focused on transport between two terminals which are linked directly [4] or through an asymmetric segment [2–4], our setup placed all nodes and their connections on an equal footing [11–13], thus enabling extending rectification studies to networks with complex topologies and geometries.

Based on our recent work [16], here we study the effect of added time-periodic modulation. Our model system is a class of spring-mass networks where each mass is subject to time-modulated Lorentz force [17,18] and is immersed in an active bath [19]. Using numerical calculations, we show that the time-modulated system is able to rectify energy fluxes between nodes and the bath. In other words, our model can act as a many-body energy pump despite the absence of temperature biases. As a comparison, our previous unmodulated system [16] supports net energy transport between sites but not between sites and baths. The modulation thus expands the toolbox for manipulating energy transport in complex networks.

We capture the numerical results by developing an analytic framework to understand the energy rectification in complex networks under time-periodic modulations. We first expand the energy flux with respect to the modulation amplitude using the Martin-Siggia-Rose–Janssen–De Dominicis–Peliti (MSR-JDP) path integral formalism [20–22], which reveals the mechanism for energy pumping through a modulation-induced coupling between different Fourier modes of the response function. We further perform a diagrammatic expansion with respect to the interaction strength using techniques we developed in Ref. [16], which provides a way to understand rectification in complex networks from local sub-networks. We can then engineer flux patterns by designing local building blocks. As a rule of thumb, roughly the more neighbors a node has, the more energy it receives from other nodes. Taken together, we demonstrated modulation-induced energy pumping in complex network systems, and developed a theoretical framework to understand the mechanism and organization of the energy rectification. The rectification principle improves our understanding of energy transport and its control in complex systems.

The remainder of this manuscript is organized as follows. In Sec. II, we introduce our time-modulated active gyroscopic model, provide a microscopic definition for the energy flux, and present numerical results. In Secs. III–V we develop a theoretical framework for the energy flux that combines path integral formalism and a diagrammatic approach. In Sec. VI we utilize the rectification principle to engineer flux patterns.

II. MODEL SYSTEMS AND ENERGY PUMPING

The equation of motion for our modulated active gyroscopic network model [Fig. 1(a)] reads [16]

$$m\dot{v}_i = -k_g z_i + \sum_j F_{ji} - \hat{B}(t)A_1 v_i - \gamma v_i + \eta_i. \quad (1)$$

We used $z_i \equiv (x_i \ y_i)^T$ to denote the displacement of particle i from its mechanical equilibrium position. Similarly v_i and η_i denote the velocity and the noise. $-k_g z_i$ is an on-site tether-

---

*Present address: Interdisciplinary Center for Brain Information, Shenzhen Institutes of Advanced Technology, Chinese Academy of Sciences, Shenzhen 518055, China; zh.liao@siat.ac.cn
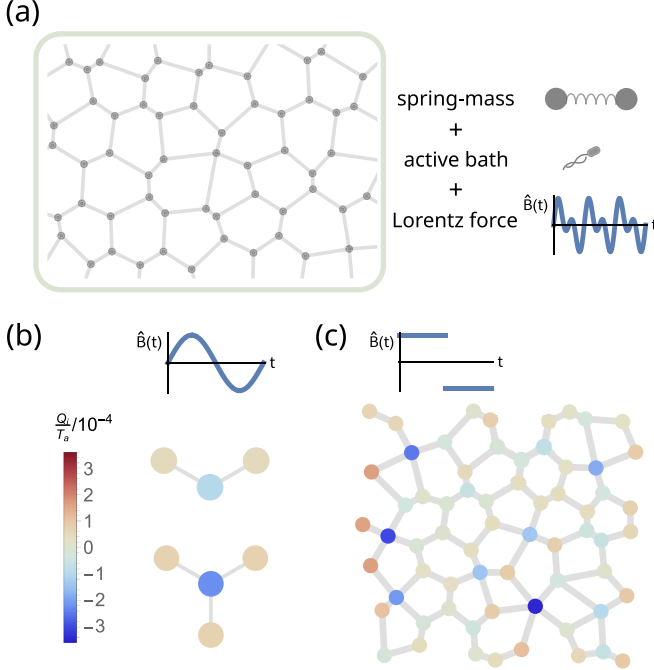
†Corresponding author: svaikunt@uchicago.edu

FIG. 1. Model and energy flux in example networks. (a) Schematic of the model—a spring-mass network where each particle is subject to a time-modulated Lorentz-like force and active bath. (b) Energy transferred during each period, Q_i, for networks with shape V and Y. Positive value corresponds to net energy transferred from the bath to the node. Protocol for B-field modulation is $\hat{B}(t) = \sin 2\pi t/T$, where T is the period of modulation. (c) Energy flux for disordered network subject to a step function protocol $\hat{B}(t) = 1$ if $t < T/2$, $\hat{B}(t) = -1$ if $t \geqslant T/2$. Numerical calculations were performed with all parameters set to 1. The color scale bar applies to both (b) and (c).

ing force. The linearized spring force from particle j to i is calculated as $F_{ji} = k(e_{ij}^T z_i + e_{ji}^T z_j)(-e_{ij})$, where e_{ij} is the unit vector that points from the equilibrium position of i to that of j. Time-modulated Lorentz force is $-\hat{B}(t)A_1 v_i = -\hat{B}(v_{i,y} - v_{i,x})^T$, where $\hat{B} = eB$ is the product of the electric charge e and the magnetic field B, and the matrix $A_1 \equiv \begin{pmatrix} 0 & 1 \\ -1 & 0 \end{pmatrix}$. The last two terms are the friction $-\gamma v_i$ and an Ornstein-Uhlenbeck (OU) colored noise η_i [19] from an active bath. The correlation of the OU colored noise reads

$$\left\langle \eta_i(t)\eta_j^T(t') \right\rangle = I\delta_{ij} \frac{\gamma T_a}{\tau} e^{-\frac{|t-t'|}{\tau}}, \qquad (2)$$

where τ is the correlation time, T_a controls the variance of the colored noise, and I is the identity matrix with appropriate dimensions. The friction $-\gamma v_i$ and the OU noise η_i drive the system out of equilibrium via breaking the fluctuation-dissipation relation. As a result of the periodically modulated B field, the system would reach a time-periodic steady state.

The observable we focus on is the energy transport between particles and baths at the time-periodic steady state. For a system with pairwise interactions and on-site potentials, the energy transferred from bath to particle i in each period T,

averaged over noise realizations, reads

$$Q_i = \int_0^T dt \langle q_i(t)\rangle, \quad q_i(t) = -\gamma v_i(t)^T v_i(t) + v_i(t)^T \eta_i(t). \qquad (3)$$

The first term $(-\gamma v_i^T v_i)$ measures the energy loss from the particle to the bath due to friction or dissipation. The second term $(v_i^T \eta_i)$ measures the energy gain for the particle due to fluctuating forcing from the bath. Equation (3) is derived using stochastic energetics [23,24] and a detailed procedure is described in Appendix A in Ref. [16].

The immediate consequence of time periodicity is that the total energy transfer during each period is zero, $\sum_{i=1}^N Q_i = 0$, where N is the number of particles in the system. In nonequilibrium conditions, there seems to be no further constraint on the value of each Q_i; thus there is the possibility that individual Q_i's are nonzero. Nonzero Q_i's mean that energy is rectified or pumped from some sites to the others.

Starting from the linearized equations (1), we numerically solve the time-dependent covariance matrix, from which we calculate Q_i [25,26] (Appendix A). Figures 1(b) and 1(c) show a collection of numerical results for small and larger networks under two example protocols for $B(t)$—a sinusoidal function and a step function. We see that there is energy pumping from some sites to the others. A more detailed description of the average (but not dynamical) picture is as follows: Energy is transferred from bath to particles labeled by $Q_i > 0$, transmitted through the bonds in the network, and released from particles labeled by $Q_i < 0$ to their surrounding bath. If we were to view this phenomenon from the perspective of conventional temperature-driven transport, we see that, although all particles are subject to the same bath or environment, some sites appear *as if* they were hotter ($Q_i > 0$) or colder ($Q_i < 0$).

Conventional transport theories cannot explain the mechanism of such energy pumping. Moreover, the energy is pumped between multiple sites of the network, contrasting conventional transports between only two terminals. It would be beneficial to develop a theory to capture such kind of transport between multiple sites, and, specifically, explain how the pumping depends on the structure of complex networks.

We shall briefly comment on the necessity of colored noise and the choice of modulating the B field. If one assumes white noise, the system would remain in Boltzmann distribution and thus no energy pumping regardless of the time-varying B field, which can be seen from the Bohr–van Leeuwen theorem [27] or the Fokker-Planck equation. Modulation of the B field as opposed to other parameters does not directly alter the energy or energy transfer. By contrast, a sudden decrease in spring constant would cause "spurious" energy loss.

III. THEORY OUTLINE: A TWO-STEP PERTURBATION STRATEGY

We outline a two-step perturbation theory that aims to explain the emergence of energy fluxes and the connection of fluxes to local properties. Details of each step will be discussed in the next two sections. This two-step strategy is motivated by our recent work on networks under constant B fields [16], where we developed a diagrammatic approach as
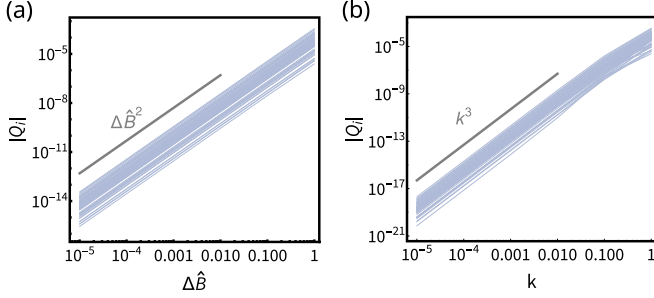
(a)

(b)

FIG. 2. Scaling of energy flux with respect to (a) $\Delta\hat{B}$ and (b) k for the disordered network as in Fig. 1(c). Each single curve is the scaling for one node. The modulation protocol is a step function that switches between $\Delta\hat{B}$ and $-\Delta\hat{B}$ with period 1. All other parameters are set to 1.

an efficient way to connect transport behavior to local properties. However, the diagrammatic approach cannot directly be applied to the time-modulated case here because its central quantity, the response function, would be invalid.

To overcome this obstacle, in the first step, we treat the time modulation as a perturbation and relate the perturbed system to the unperturbed ones. We write the time-modulated B field as $\hat{B}(t) = \hat{B} + \Delta\hat{B}(t)$, where $\hat{B}$ is a time-independent reference field and $\Delta\hat{B}(t)$ is a time-periodic modulation with a perturbative amplitude. Using the Martin-Siggia-Rose–Janssen–De Dominicis–Peliti (MSR-JDP) path integral formalism [20–22], correlators under a time-periodic system can be expressed in terms of correlators under a time-invariant reference system. We will see in Eq. (15) that the response matrix at different Fourier frequencies gets coupled, which is the main mechanism behind the emergence of the energy flux.

In the second step, we are ready to apply a diagrammatic approach similar to Ref. [16]. We perform an expansion with respect to interactions or the spring constant and express the energy transfer as intuitive diagrams. These diagrams then enable us to relate the energy flux in complex networks to the structure of local subnetworks.

Numerical results in Fig. 2 show that to the lowest non-vanishing order $Q_i \sim \Delta\hat{B}(t)^2 k^3$. These observations suggest a goal for analytical efforts, which is to develop an expression to the order of $\Delta\hat{B}(t)^2 k^3$, explain why lower order terms vanish, and more importantly explore properties of energy pumping on this nonvanishing order. We also observed fluxes whose leading order terms are higher than $\Delta\hat{B}(t)^2$ or k^3 in networks with higher symmetries. These networks are special cases and thus are not our focus.

IV. PERTURBATIVE EXPANSION IN THE MODULATION: A MSR-JDP APPROACH

A. MSR-JDP path integral formalism

The Martin-Siggia-Rose–Janssen–De Dominicis–Peliti (MSR-JDP) path integral formalism [20–22,28] is a powerful framework for studying statistical properties, e.g., the average of an observable O, of a stochastic trajectory when compared with another trajectory. Applying to our system, the former trajectory is one under modulated B field, in which the average is denoted as $\langle O \rangle_{B_t}$, and the latter is one under constant B

field, in which the average is denoted as $\langle O \rangle$. The average $\langle O \rangle_{B_t}$ can be expressed as a path integral

$$\langle O \rangle_{B_t} = \int \mathcal{D}z\mathcal{D}v\mathcal{D}\eta \, O\mathcal{N} \prod_t \delta(\dot{z} - v)\delta(m\dot{v}$$
$$+ Kz + k_g z + \gamma v + \hat{B}(t)Av - \eta)\mathcal{P}[\eta], \quad (4)$$

where the Dirac-δ functions ensure that the equations of motion are satisfied, $\mathcal{P}[\eta]$ is the probability of the noise, and $\mathcal{N}$ is the normalization constant. We have expressed the N-particle system using $2N$-dimensional column vectors, e.g., $z = \sum_i |i\rangle \otimes z_i$, where $|i\rangle$ denotes the 2D subspace corresponding to particle i. The matrix K calculates interparticle spring forces F_s due to particles' displacements, $F_s = -Kz$. The matrix $A = \sum_i |i\rangle\langle i| \otimes A_1$.

The modulated B field can be decomposed into a constant part and a (potentially perturbative) time-varying part, $\hat{B}(t) = \hat{B} + \Delta\hat{B}(t)$. Contributions to the path integral from these two parts can be separated via the introduction of an auxiliary field $iu = \sum_i |i\rangle \otimes iu_i$ through $\delta(\hat{B}Av + \Delta\hat{B}(t)Av + \cdots) \propto \int du \, e^{-iu^T(\hat{B}Av + \cdots)} e^{-iu^T[\Delta\hat{B}(t)Av]}$. Further notice that when $\Delta\hat{B} = 0$ the path integral Eq. (4) reduces to $\langle O \rangle$. We get

$$\langle O \rangle_{B_t} = \left\langle O \, e^{-\int dt \, \Delta\hat{B}_t iu^T Av} \right\rangle, \quad (5)$$

where we have written the time variable in subscripts for simplicity. In regimes where the amplitude of $\Delta B(t)$ is small, the right hand side can be expanded,

$$e^{-\int ds \, \Delta\hat{B}_s iu^T Av} = 1 - \int ds \, \Delta\hat{B}_s iu_s^T Av_s$$
$$+ \frac{1}{2}\int ds \, ds' \left(\Delta\hat{B}_s iu_s^T Av_s\right)\left(\Delta\hat{B}_{s'} iu_{s'}^T Av_{s'}\right)$$
$$- \cdots . \quad (6)$$

In Eqs. (5) and (6), we have used the MSR-JDP framework to express the average under modulated conditions in terms of some other average under unmodulated conditions.

The observable we are interested in is the energy flux from the bath to the particle, Eq. (3). To account for the site index more conveniently, we use a projection operator P_i,

$$P_i = |i\rangle\langle i| \otimes \begin{pmatrix} 1 & 0 \\ 0 & 1 \end{pmatrix}, \quad (7)$$

and rewrite the flux quantity $q_i(t)$ as

$$q_i(t) = -\gamma (P_i v_t)^T P_i v_t + (P_i v_t)^T P_i \eta_t. \quad (8)$$

Combining Eq. (8) with the expansion Eq. (6), we obtain expressions for the pumped energy to different orders in ΔB,

$$\langle Q_i^{(0)} \rangle_{B_t} = \int_0^T dt \langle q_i(t) \rangle, \quad (9)$$

$$\langle Q_i^{(1)} \rangle_{B_t} = -\int_0^T dt \, ds \langle q_i(t)\Delta\hat{B}_s iu_s^T Av_s \rangle, \quad (10)$$

$$\langle Q_i^{(2)} \rangle_{B_t} = \frac{1}{2}\int_0^T dt \, ds \, ds' \langle q_i(t)\left(\Delta\hat{B}_s iu_s^T Av_s\right)$$
$$\times \left(\Delta\hat{B}_{s'} iu_{s'}^T Av_{s'}\right)\rangle. \quad (11)$$

Here we write down the expansion to quadratic order because, as we will show in the next subsection, the zeroth order and the linear order terms vanish.

To calculate the explicit expressions from Eqs. (9)–(11), one requires the evaluation of two-point correlators and multipoint correlators. The two-point correlators can be expressed in terms of spectral response function $G^+(\omega)$ for the reference system under constant B,

$$G^\pm(\omega) = [K + k_g I \pm i\omega(\gamma I + \hat{B}A) - m\omega^2 I]^{-1}. \quad (12)$$

The Fourier transform is defined as $\tilde{f}(\omega) = \int_{-\infty}^{\infty} dt\, f(t) e^{-i\omega t}$. The response function describes how the system responds to fluctuations $\tilde{z}(\omega) = G^+(\omega)\tilde{\eta}(\omega)$. Explicit expressions of relevant two-point correlators are presented in Appendix B 1. The multipoint correlators can be written as combinations of two-point correlators via Wick's theorem [29].

To make our theory more general, we introduce a function $h(\omega)$ to describe a generic noise spectrum

$$\langle \tilde{\eta}(\omega)\tilde{\eta}(\omega')^T \rangle = 2\gamma T_a h(\omega) 2\pi \delta(\omega + \omega') I. \quad (13)$$

For white noise, $h(\omega)$ is constant. For the OU colored noise described in Eq. (2), $h(\omega) = 1/(1 + \omega^2\tau^2)$.

The time-periodic modulation $\Delta\hat{B}(t)$ will be represented by its Fourier series with coefficients $\Delta\tilde{B}_n$,

$$\Delta\hat{B}(t) = \sum_{n=-\infty}^{\infty} \Delta\tilde{B}_n e^{i\omega_n t}, \quad \omega_n = \frac{2\pi n}{T}, \quad (14)$$

where $n = \ldots, -1, 0, 1, \ldots$ and $\Delta\tilde{B}_n = \Delta\tilde{B}_{-n}^*$.

B. Zeroth and the linear order flux vanish

The zeroth order modulation corresponds to a constant B field. This case has been explored previously, which showed that there is no net energy flux between the bath and the particle, $\langle Q_i^{(0)} \rangle_{B_t} = \int_0^T dt\, \langle q_i(t) \rangle = 0$ (Appendix C in Ref. [16]).

One may expect that the linear order flux also vanish, because sin-wave modulation and its opposite, $-\sin$, should result in the same periodic steady state. However, this argument does not account for modulations that consist of multiple sinusoidal waves. Through explicitly calculating the linear order energy flux, we show that different modes of modulation are decoupled; thus the linear order term also vanishes (Appendix B 2).

C. Quadratic order flux explains pumping mechanism

There is no *a priori* reason for quadratic order energy flux to vanish. Starting from the expression for $\langle Q_i^{(2)} \rangle_{B_t}$, Eq. (11), we calculate the six-point correlators and get (details in Appendix B 3)

$$\langle Q_i^{(2)} \rangle_{B_t} = 4\gamma T_a T \sum_{n=1}^{\infty} |\Delta\tilde{B}_n|^2 \int \frac{d\omega}{2\pi}$$
$$\times \{\omega^2(\omega + \omega_n)[h(\omega + \omega_n) - h(\omega)]$$
$$\times \text{Re}[i\, \text{tr}\, P_i G^+(\omega)AG^+(\omega + \omega_n)AG^+(-\omega)^T]\}.$$
$$(15)$$

This theoretical expression can explain how energy pumping is generated in the presence of the colored noise and the modulation.

The role of the colored noise takes effect through the factor $h(\omega + \omega_n) - h(\omega)$. If the noise spectrum $h(\omega)$ is flat, which corresponds to a white noise, this factor vanishes. Only colored noise with nonflat spectrums can generate a nonzero $\langle Q_i^{(2)} \rangle_{B_t}$.

The role of modulated B field is to induce couplings between different modes of the response function, which is manifest through the factor $G^+(\omega)AG^+(\omega + \omega_n)AG^+(-\omega)^T$. This is in contrast with the unmodulated case where $G^+(\omega)$ at different frequencies are uncoupled, which leads to no pumping [16]. Thus the coupling between different modes is one necessary mechanism for energy pumping in our model.

Another flux property related to the modulation is that contributions from different terms in the Fourier series of $\Delta B(t)$ are independent, which can be seen from the summation $\sum_{n=1}^{\infty} |\Delta\tilde{B}_n|^2(\cdots)$. As a consequence, we only need to discuss the flux from each mode of $\Delta B(t)$. Then the flux for arbitrary modulation protocols can be obtained by weighted combinations of the individual modes.

V. FURTHER EXPANSION IN THE INTERACTION: A DIAGRAMMATIC APPROACH

A. Diagrammatic expansion and two useful properties

Having explained the mechanism of energy pumping, we now study detailed properties of the flux, in particular, the relationship between flux pattern in a complex network and the structure of local subnetworks. When interactions are weak, it can be expected that the flux for a node mainly depends on its immediate surroundings. The diagrammatic approach provides a tool to explicitly find such dependence.

Starting from the expression (15), we expand the response functions with respect to small k into products of the noninteracting part (matrix $G^+|_{k=0}$) and the interacting part (matrix K). Due to the pairwise spring-mediated interactions, the matrix K has a block structure, which depends on the topology and the geometry of the network. Further expansion based on the blocks results in terms that can be pictorially represented as diagrams and are closely related to the network structure. Diagrams for the energy flux between site i and the bath are paths that start from i, iteratively step to bonded neighbors or to the site itself, and finally end at site i. Diagrams with $|l|$ steps correspond to mathematical expressions that are on the order of $k^{|l|}$, which we will denote as $|l|$'s order diagrams. In the small-k regime a lower-order diagram contributes more to the flux. The mathematical expression corresponding to each diagram is lengthy, which we present in Appendix C 1.

We point out two useful properties of the diagrams. The first property is that if there is no loop on a site, then the diagram is equivalent to a simplified one where all other branches on the site are removed [Fig. 3(a), Appendix C 1]. The second property is that if a diagram consists of solely loops, its value vanishes [Fig. 3(b), Appendix C 2]. As we saw from numerical results in Fig. 2, energy fluxes scale as k^3. Using the two properties described above, we will show
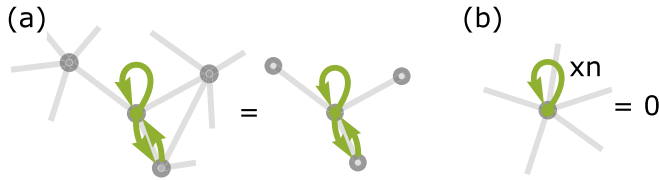
FIG. 3. Two useful properties of the diagrams. The starting and ending site is labeled in green. (a) If there is no loop on a site, then the diagram is equivalent to a simplified one where all other branches on the site are removed. (b) Diagrams consisting of only loops vanish. The symbol n in the figure represents an arbitrary number.

in the following two subsections why lower order diagrams vanish and how the third order diagrams reveal an explicit relationship between fluxes in complex networks and local structures.

B. First and second order diagrams vanish

The first order diagrams mean those with only one step. The only possible first order diagrams are those with one loop on the node. According to the second property, all first order diagrams vanish.

Second order diagrams also vanish for the following reason. The second order diagrams for site i have the form $i \rightarrow j \rightarrow i$, where j's are the bonded neighbors [Fig. 4(a); diagrams with only loops are eliminated]. Using property one, these diagrams are equivalent to the diagram $1 \rightarrow 2 \rightarrow 1$ in a network that consists of only two nodes, 1 and 2. From symmetry, the flux in the two-node network is zero. At the k^2 level, this means that the sum of a looped diagram and a $1 \rightarrow 2 \rightarrow 1$ diagram is zero [Fig. 4(b)]. Thus the $1 \rightarrow 2 \rightarrow 1$ diagram and equivalently $i \rightarrow j \rightarrow i$ diagrams vanish.

C. Third order diagrams reveal connection between flux and local properties

The third order diagrams do not vanish in general. Investigation of the third order diagrams shows how the flux in a complex network can be represented using local properties.

In Fig. 5(a), we write down all diagrams for a node in arbitrary networks. The network fragment in Fig. 5(a) is representative of all possible connections surrounding a node
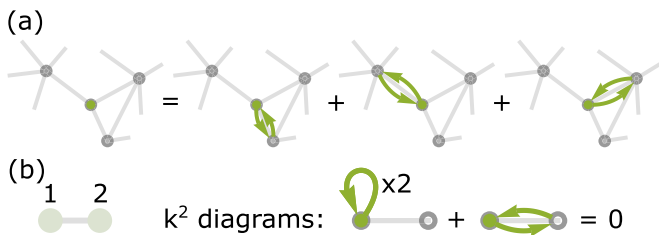

FIG. 4. Second order diagrams vanish. (a) Diagrammatic expansion of the energy flux on the order of k^2. Diagrams with only loops are eliminated. From property one, these $i \rightarrow j \rightarrow i$ diagrams are equivalent to the $1 \rightarrow 2 \rightarrow 1$ diagram in a two-node network. (b) In the two-node network, the sum of diagram $1 \rightarrow 1 \rightarrow 1$ and diagram $1 \rightarrow 2 \rightarrow 1$ is zero. Using property two, the diagram $1 \rightarrow 2 \rightarrow 1$ vanishes.

i, which include bondings between i and its neighbors j's, bondings between two of its neighbors, and bondings between its neighbors and other nodes in the network. The flux on the generic node i from the third order equals the sum of all third order diagrams.

All third order diagrams can be classified into three classes and then simplified using property one. The first class of diagrams contain a loop on node i, such as $i \rightarrow i \rightarrow j \rightarrow i$, $i \rightarrow j \rightarrow i \rightarrow i$. The sum of all class one diagrams is equal to the third order flux of node i in a trimmed subnetwork centered around i, where all neighbors of j and all connections between j's are removed. The second class of diagrams contain a loop on node j, e.g., $i \rightarrow j \rightarrow j \rightarrow i$. Each diagram in class two is equal to the flux of node i in a trimmed subnetwork centered around j. The third class of diagrams are triangles that contain arrows between bonded j's, e.g., $i \rightarrow j_1 \rightarrow j_2 \rightarrow i$. The above classification shows an explicit relation between fluxed in complex networks and local properties, which is depicted in Fig. 5(b).

If a network does not contain any triangular connections, then its flux can be obtained by summing over trimmed subnetworks of the first two classes. A consequence is that we can simply reconstruct the flux in large-scale networks from small subnetworks. Figure 6 is a numerical demonstration that such reconstructed fluxes match well with the original ones.

VI. UTILIZING LOCAL BUILDING BLOCKS TO CREATE COMPLEX PATTERNS OF ENERGY TRANSPORT

The connection between flux in a network and in its local subnetworks can be exploited to create complex patterns of energy transport. If we assume that the energy in the bath diffuses slowly, then energy fluxes can lead to temperature changes, which means that our setup could potentially be used to engineer temperature inhomogeneities using homogeneous modulations.

The objective can be posed as follows: given a grid of unconnected nodes and a target pattern, we design connections between the nodes such that the consequent flux pattern matches a target one. From the relation between flux in complex networks and its local structures (Sec. V C), we can inversely use the local subnetworks as building blocks. The building blocks considered here are star-shaped networks with one central node and a number of evenly spaced neighbors. Figure 7(a) shows that the flux of the central node increases in its magnitude as the number of branches increases. Based on this observation, we can create connections simply by considering the difference between the degree of a node and degrees of its neighbors. Consider a target drawing that consists of a white background and darker patterns; we first highlight nodes corresponding to darker pixels in the pattern. Then for each highlighted node we create connections to nonhighlighted ones with angles as even as possible. The degree of a highlighted node is proportional to the darkness of its corresponding pixel. The average degree of nonhighlighted nodes, due to their larger population, is smaller than that of the highlighted ones. We avoid connections between highlighted nodes or between nonhighlighted nodes, in order to avoid influence from triangle diagrams. Note that the connections built from this strategy can be long ranged in space. In Fig. 7(b)
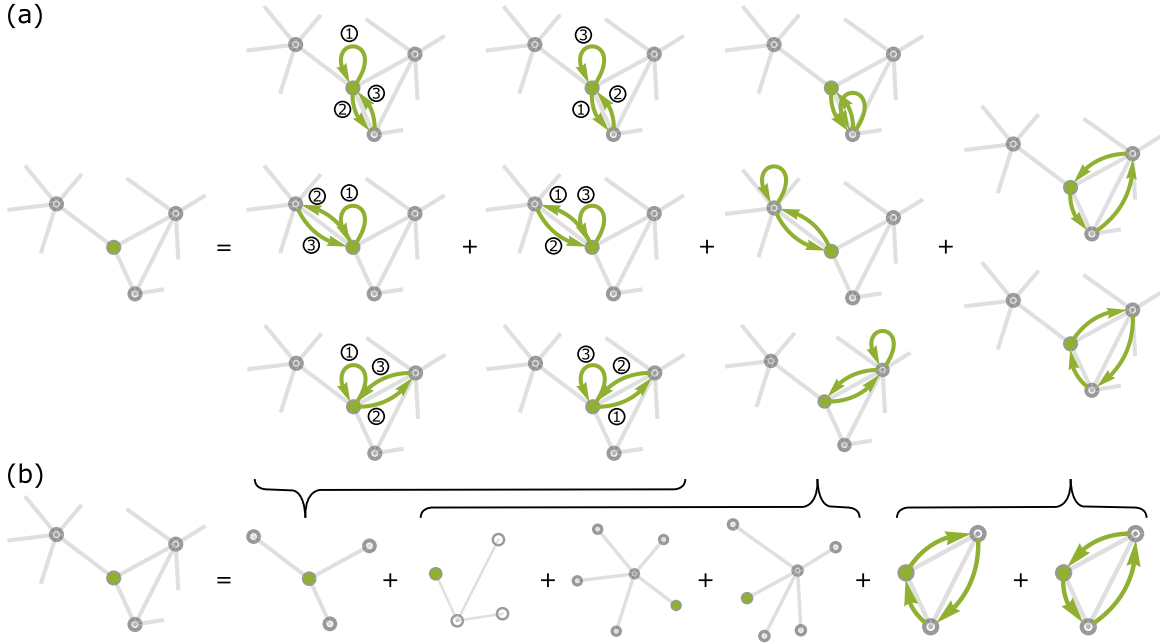
FIG. 5. Third order diagrams for a node in arbitrary networks. (a) All third order diagrams for the node labeled in green. The number in circles labels the order in the path. (b) These diagrams or their partial sums can be classified into three groups and then simplified. The third order flux of the labeled node is equal to the sum of fluxes of corresponding nodes in trimmed subnetworks and fluxes of triangle diagrams.

we demonstrate the pattern of a gray-scaled book constructed through the above strategy. It may be possible to achieve a broader range of patterns or avoid long-ranged connections using other strategies.

The observed relation between flux amplitude and the number of branches [Fig. 7(a)] can be quantified and explained by our diagrammatic theory in the perturbative regime. For a star-shaped network with evenly spaced branches, the flux of the central node, Q_c, is proportional to the square of the number of branches, N. A brief explanation of the flux scaling is as follows. For the flux on a side node, $Q_s(= -Q_c/N)$, the contribution comes from the diagram $side \rightarrow center \rightarrow center \rightarrow side$ (other diagrams vanish). Due to the loop on the center, the value of the diagram depends on the force response of the central node, which increases linearly with the number of its neighbors (for $N \geqslant 3$). As a result, $Q_s \propto N$, $Q_c = -NQ_s \propto$

N^2 (see Appendix D for details). Using evenly spaced star-shaped building blocks to approximate more irregular ones, we obtain a pattern that roughly the more neighbors a node has (compared with degrees of its neighbors), the "colder" ($Q_i < 0$) it is [Figs. 1(b) and 1(c)].

VII. CONCLUSION

In conclusion, we have constructed an active gyroscopic network model where the B field is modulated in a time-periodic manner. We numerically demonstrated that our model is able to rectify energy transport between nodes and baths in the absence of any temperature biases. Importantly, by combining the MSR-JDP formalism and our diagrammatic
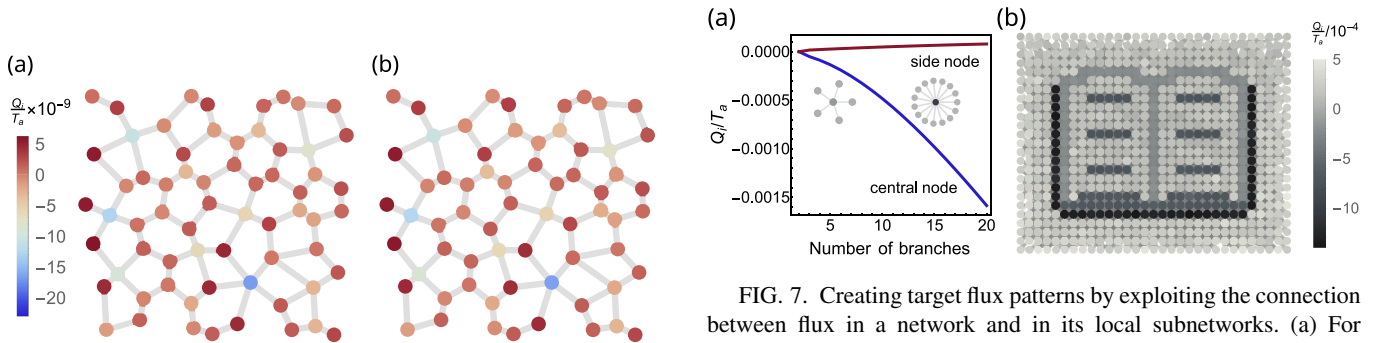

FIG. 6. Energy fluxes reconstructed from local subnetworks match well with the original ones. (a) Fluxes calculated from the full network. (b) Fluxes calculated from local subnetworks then combined according to reconstruction rules. The system and the modulation protocol are mostly the same as in Fig. 1(c) except that $\Delta \hat{B} = 0.1$, $k = 0.1$. The color scale bar applies to both (a) and (b).

FIG. 7. Creating target flux patterns by exploiting the connection between flux in a network and in its local subnetworks. (a) For star-shaped networks with parameters specified below, the flux amplitude of the central node increases with the number of branches. (b) Constructed network and its flux pattern that mimics a grayscaled book. The modulation is a step function where $\hat{B}(t)$ switches between -1 and 1. The period is taken to be infinite so that steady states are reached before $\hat{B}(t)$ changes its value. All parameters are set to 1 except $k = 0.05$.

approach, we formulate a connection between flux pattern in complex networks and the flux pattern in local subnetworks. Such connection enables us to understand and control energy pumping in arbitrary complex networks. In particular, we can engineer flux patterns by designing building blocks, for example, by connecting a desired "colder" node with more neighbors. The combined MSR-JDP and diagrammatic approach can in principle be applied to calculate generic correlators for perturbed linear networks with arbitrary geometry and topology.

APPENDIX A: NUMERICAL CALCULATION OF ENERGY FLUX FROM TIME-DEPENDENT COVARIANCE MATRIX

We first consider the evolution of our active gyroscopic network under a constant B field. Then we numerically approximate the time-varying B field by discretizing it into short segments, each under a constant B.

Under constant B field, the evolution of our system as described in the extended space $X = \{z, v, \eta\}$ obeys linear dynamics. Here the Ornstein-Uhlenbeck colored noise is treated by the evolution [19]

$$\tau \dot{\eta}_i = -\eta_i + \sqrt{2\gamma T_a}\xi_i. \tag{A1}$$

For a general linear stochastic equation with time-independent drift μ and diffusion factor σ,

$$dX = \mu\, dt + \sigma\, dW, \tag{A2}$$

its steady-state covariance matrix $C = \langle XX^T \rangle$ can be numerically solved from the matrix equation $-(\mu C + C\mu^T) = \sigma\sigma^T$ [25,26]. The evolution of the covariance $C(t)$ starting from an initial state C_0 reads

$$C(t) = C + e^{\mu t}(C_0 - C)e^{\mu^T t}. \tag{A3}$$

From $C(t)$ we can extract the energy flux, $q_i(t) = -\gamma v_i^T v_i + v_i^T \eta_i$, and subsequently calculate its time integral.

Our numerical procedure to calculate Q_i is as follows. Given a protocol $B(t)$, we discretize it into short segments in time. In each segment the B field is constant and is evaluated at the starting time of that segment. Consequently, the covariance matrix in each segment can be calculated using Eq. (A3). The evolution $C(t)$ for protocol $B(t)$ can thus be solved by combining results from all segments. We choose a starting C_0 to be the steady state under constant $B(0)$ and evolve $C(t)$ for many periods until $C(nT) - C(nT + T)$ is smaller than target numerical precision, which indicates that the time-periodic steady state is achieved. Then we evolve $C(t)$ from this steady state and calculate the pumped energy Q_i. The source of numerical errors mainly come from discretization. Numerical calculations are performed using Mathematica with custom code.

APPENDIX B: PERTURBATIVE EXPANSION IN MODULATED *B* FIELD

1. Two-point correlators expressed in terms of the response function

Correlators relevant to calculating $\langle Q_i^{(1)} \rangle_{B_t}$ and $\langle Q_i^{(2)} \rangle_{B_t}$ involve v_t, η_t, iu_t (but not z_t). In this Appendix, we express the relevant two-point correlators in terms of the response function $G^+(\omega)$.

Correlators that do not involve the auxiliary field iu_t can be calculated directly. We show an example calculation of the correlator $\langle v_t v_s^T \rangle$,

$$\langle v_t v_s^T \rangle = \int \frac{d\omega}{2\pi} e^{i\omega(t-s)}(i\omega)(-i\omega)2\gamma T_a h(\omega)G^+(\omega)G^-(\omega)^T \tag{B1}$$

$$= \int \frac{d\omega}{2\pi} e^{i\omega(t-s)} i\omega T_a h(\omega)[G^+(\omega) - G^{-T}(\omega)], \tag{B2}$$

where to reach the second line we have used $G^{-T} - G^+ = 2i\omega\gamma G^+ G^{-T}$ [30].

To calculate correlators that involve the auxiliary field, we first need to review the connection between the auxiliary field and the response of the system. Consider an unmodulated system that is perturbed by an external force $f(t)$,

$$m\dot{v} = -Kz - \gamma v - \hat{B}Av + \eta + f. \tag{B3}$$

The MSR-JDP result can be obtained by simply replacing $-\Delta\hat{B}Av$ in Eq. (5) by f, which reads

$$\langle O \rangle_f = \langle O\, e^{\int dt\, iu^T f} \rangle. \tag{B4}$$

The correlators can then be related to the response

$$\langle Oiu_{i,s} \rangle = \left. \frac{\delta}{\delta f_{i,s}} \langle O \rangle \right|_{f \to 0}, \tag{B5}$$

$$\langle Oiu_{i,s}iu_{i',s'} \rangle = \left. \frac{\delta}{\delta f_{i,s}\delta f_{i',s'}} \langle O \rangle \right|_{f \to 0}, \tag{B6}$$

where we have expressed the component of the vector f, iu explicitly. From the above expressions we see that these correlators are connected to responses to an external perturbation, for which reason the auxiliary field iu is also called a response field. For our linear reference system, such response can be expressed in terms of the response function $G^+(\omega)$.

The two-point correlators needed to calculate $\langle Q_i^{(1)} \rangle_{B_t}$ and $\langle Q_i^{(2)} \rangle_{B_t}$ are summarized as follows:

$$\langle v_t v_s^T \rangle = \frac{1}{2\gamma}\left(\langle v_t \eta_s^T \rangle + \langle v_s \eta_t^T \rangle^T\right), \tag{B7}$$

$$\langle v_t \eta_s^T \rangle = 2\gamma T_a \int \frac{d\omega}{2\pi} e^{i\omega(t-s)} i\omega h(\omega)G^+(\omega), \tag{B8}$$

$$\langle \eta_t \eta_s^T \rangle = 2\gamma T_a \int \frac{d\omega}{2\pi} e^{i\omega(t-s)} h(\omega), \tag{B9}$$

$$\langle v_t iu_s^T \rangle = \int \frac{d\omega}{2\pi} e^{i\omega(t-s)} i\omega G^+(\omega), \tag{B10}$$

$$\langle \eta_t iu_s^T \rangle = 0, \tag{B11}$$

$$\langle iu_t iu_s^T \rangle = 0. \tag{B12}$$

2. Linear order perturbation in modulation

In this Appendix, we derive the linear order energy flux with respect to modulation of the B field. We show that this contribution vanishes.

From Eqs. (10) and (8), the linear order energy flux reads

$$\langle q_i(t)^{(1)}\rangle_{B_t} = -\int ds\, \Delta\hat{B}_s\big\{\langle -\gamma (P_i v_t)^T P_i v_t i u_s^T A v_s\rangle$$
$$+ \langle (P_i v_t)^T P_i \eta_t i u_s^T A v_s\rangle\big\}. \tag{B13}$$

Using Wick's theorem for four-point correlators,

$$\langle a^T b c^T d\rangle = \text{tr}\langle ab^T\rangle \text{tr}\langle cd^T\rangle + \text{tr}\langle ac^T\rangle\langle db^T\rangle$$
$$+ \text{tr}\langle ad^T\rangle\langle cb^T\rangle, \tag{B14}$$

the first and the second term in Eq. (B13) are reduced to

$$-\gamma\langle (P_i v_t)^T P_i v_t i u_s^T A v_s\rangle = -\gamma(\text{tr}\, P_i\langle v_t v_t^T\rangle \text{tr}\, A\langle v_s i u_s^T\rangle$$
$$+ 2\,\text{tr}\, P_i\langle v_t i u_s^T\rangle A\langle v_s v_t^T\rangle), \tag{B15}$$

$$\langle (P_i v_t)^T P_i \eta_t i u_s^T A v_s\rangle = \text{tr}\, P_i\langle v_t \eta_t^T\rangle \text{tr}\, A\langle v_s i u_s^T\rangle$$
$$+ \text{tr}\, P_i\langle v_t i u_s^T\rangle A\langle v_s \eta_t^T\rangle. \tag{B16}$$

The sum of the first terms on both right hand sides (RHSs) vanishes because

$$\big(-\gamma\,\text{tr}\, P_i\langle v_t v_t^T\rangle + \text{tr}\, P_i\langle v_t \eta_t^T\rangle\big) = \langle q_i(t)\rangle = 0. \tag{B17}$$

The sum of the second terms on both RHSs can be simplified to $-\text{tr}\, P_i\langle v_t i u_s^T\rangle A\langle v_s \eta_t^T\rangle^T$ using Eq. (B7). Plugging in expressions for correlators presented in Appendix B 1, we get

$$\langle q_i(t)^{(1)}\rangle_{B_t} = 2\gamma T_a \int \frac{d\omega}{2\pi}\frac{d\omega'}{2\pi} ds\{\Delta\hat{B}_s e^{i(\omega-\omega')(t-s)}$$
$$\times (i\omega)(i\omega')h(\omega')\,\text{tr}\, [P_i G^+(\omega) A G^+(\omega')^T]\}. \tag{B18}$$

Integration over s can be written with the Fourier transform of ΔB,

$$\int ds\, \Delta\hat{B}_s e^{i(\omega-\omega')(t-s)} = \Delta\tilde{B}(\omega-\omega')e^{i(\omega-\omega')t}. \tag{B19}$$

We then integrate over t. Since $\Delta\hat{B}(t)$ is a periodic function with period T, it can be expanded in discrete Fourier modes,

$$\Delta\hat{B}(t) = \sum_{n=-\infty}^{\infty} \Delta\tilde{B}_n e^{i\omega_n t}, \quad \omega_n = \frac{2\pi n}{T}, \tag{B20}$$

$$\Delta\tilde{B}(\omega) = \sum_n \Delta\tilde{B}_n 2\pi\delta(\omega-\omega_n), \tag{B21}$$

with the property $\Delta\tilde{B}_n = \Delta\tilde{B}_{-n}^*$. The integration over t reads

$$\int_0^T dt\, e^{i\omega_n t} = \begin{cases} T, & \text{if } \omega_n = 0, \\ \frac{1}{i\omega_n}(e^{i\omega_n T}-1) = 0, & \text{if } \omega_n \neq 0, \end{cases} \tag{B22}$$

$$= T\delta_{n,0}. \tag{B23}$$

We introduce an auxiliary function

$$f_1(\omega,\omega') = 2\gamma T_a(i\omega)(i\omega')h(\omega')\,\text{tr}\, [P_i G^+(\omega) A G^+(\omega')^T]. \tag{B24}$$

The linear order energy flux at time instant t reads

$$\langle q_i(t)^{(1)}\rangle_{B_t} = \int \frac{d\omega}{2\pi}\frac{d\omega'}{2\pi} \Delta\tilde{B}(\omega-\omega')e^{i(\omega-\omega')t} f_1(\omega,\omega') \tag{B25}$$

$$= \sum_n \int \frac{d\omega}{2\pi} \Delta\tilde{B}_n e^{i\omega_n t} f_1(\omega,\omega-\omega_n), \tag{B26}$$

which shows that different modulation modes, $\Delta\tilde{B}_n$, are decoupled.

After time integration the result reads

$$\langle Q_i^{(1)}\rangle_{B_t} = \int_0^T dt\, \langle q_i(t)^{(1)}\rangle_{B_t} \tag{B27}$$

$$= T\int \frac{d\omega}{2\pi} \Delta\tilde{B}_0 f_1(\omega,\omega) \tag{B28}$$

$$= 2\gamma T_a T\int \frac{d\omega}{2\pi}\{\Delta\tilde{B}_0 h(\omega)(i\omega)^2$$
$$\times \text{tr}\, [P_i G^+(\omega) A G^+(\omega)^T]\} = 0. \tag{B29}$$

This result shows that the only contribution is the zero-frequency mode of $\Delta\hat{B}(t)$; thus the flux should vanish. The mathematical proof is as follows: since $G^+(\omega)^T P_i G^+(\omega)$ is a symmetric matrix and A is an antisymmetric matrix, the trace of their product is zero.

3. Quadratic order perturbation in modulation

In this Appendix, we derive the expression for the quadratic order energy flux with respect to modulation of the B field, Eq. (15) in the main text. We also perform sanity checks that the energy balance is satisfied and that flux vanishes if the modulation is constant.

We start from expressions (11) and (8), and get the quadratic order energy flux at time t,

$$\langle q_i(t)^{(2)}\rangle_{B_t} = \frac{1}{2}\int ds\, ds'\langle[-\gamma(P_i v_t)^T P_i v_t + (P_i v_t)^T P_i \eta_t]$$
$$\times \big(\Delta B_s i u_s^T A v_s\big)\big(\Delta B_{s'} i u_{s'}^T A v_{s'}\big)\rangle. \tag{B30}$$

This expression involves six-point correlators, which emit 15 terms using the Wick's theorem. However, many of these terms will turn out to vanish, which greatly simplifies the calculation.

Our first task is to identify these vanishing terms. The quadratic order perturbation can be expanded as

$$\int dt\langle q_i(t)^{(2)}\rangle_{B_t} = \frac{1}{2}\int dt\, ds\, ds'\, \Delta\hat{B}_s \Delta\hat{B}_{s'}\big[\langle q_i(t)\rangle\langle i u_s^T A v_s\rangle\langle i u_{s'}^T A v_{s'}\rangle + \langle q_i(t) i u_s^T A v_s\rangle_c\langle i u_{s'}^T A v_{s'}\rangle$$
$$+ \langle i u_s^T A v_s\rangle\langle q_i(t) i u_{s'}^T A v_{s'}\rangle_c + \langle q_i(t) i u_s^T A v_s i u_{s'}^T A v_{s'}\rangle_c\big], \tag{B31}$$

where subscript "c" means the terms are "connected" inside the same trace. The first term vanishes due to $\langle q_i\rangle = 0$. The second and the third term vanish due to $\int dt\langle q_i(t)^{(1)}\rangle_{B_t} = 0$. Now we only need to consider the last term which involves the trace

connecting all six points. These terms have the form

$$\langle a^T b c^T d e^T f \rangle_c = \text{tr}\,\langle ac^T \rangle \langle df^T \rangle \langle eb^T \rangle + \text{tr}\,\langle ac^T \rangle \langle de^T \rangle \langle fb^T \rangle + \text{tr}\,\langle ad^T \rangle \langle cf^T \rangle \langle eb^T \rangle + \text{tr}\,\langle ad^T \rangle \langle ce^T \rangle \langle fb^T \rangle$$
$$+ \text{tr}\,\langle ae^T \rangle \langle fd^T \rangle \langle cb^T \rangle + \text{tr}\,\langle ae^T \rangle \langle fc^T \rangle \langle db^T \rangle + \text{tr}\,\langle af^T \rangle \langle ed^T \rangle \langle cb^T \rangle + \text{tr}\,\langle af^T \rangle \langle ec^T \rangle \langle db^T \rangle. \quad \text{(B32)}$$

Applying the above form and noticing that some two-point correlators are zero, the expression for the quadratic order energy flux Eq. (B31) simplifies to

$$\langle q_i(t)^{(2)} \rangle_{B_t} = \int ds\, ds'\, \Delta B_s \Delta B_{s'} \big\{ \text{tr}\,\big[P_i \langle v_t i u_s^T \rangle A \langle v_s \eta_{s'}^T \rangle A \langle i u_{s'} v_t^T \rangle \big]$$
$$- \text{tr}\,\big[P_i \langle v_t i u_s^T \rangle A \langle v_s i u_{s'}^T \rangle A \langle v_t \eta_{s'}^T \rangle^T \big] \big\}. \quad \text{(B33)}$$

We next plug in explicit expressions for the two-point correlators (B7)–(B12) and integrate over s, s' and t. We get

$$\langle Q_i^{(2)} \rangle_{B_t} = 2\gamma T_a T \sum_{n=-\infty}^{\infty} |\Delta \tilde{B}_n|^2 \int \frac{d\omega}{2\pi}$$
$$\times \big\{ i\omega^2(\omega - \omega_n)[h(\omega - \omega_n) - h(\omega)]$$
$$\times \text{tr}\, P_i G^+(\omega) A G^+(\omega - \omega_n) A G^+(-\omega)^T \big\}. \quad \text{(B34)}$$

It can be shown that the ω_n term and the $-\omega_n$ term form a complex conjugate pair. From this property and Eq. (B34), we reach the final expression for the quadratic order energy flux (15) in the main text.

APPENDIX C: FURTHER PERTURBATIVE EXPANSION IN INTERACTION

1. Procedure and result of the diagrammatic approach

The diagrammatic approach is built on an expansion of the response function. We first review the diagrammatic expansion of a single response function [16], then combine the three response functions and other parts in Eq. (15) or Eq. (B34) to get the diagrammatic expression for the energy flux.

In the small-k regime, the response function $G^+(\omega)$ [Eq. (12)] can be expanded as

$$G^+ = \frac{1}{(G^+|_{k=0})^{-1} + K} = \sum_{|l|=0} G^+|_{k=0}[(-K)G^+|_{k=0}]^{|l|}. \quad \text{(C1)}$$

The noninteracting part $G^+|_{k=0}$ is block diagonal: $G^+|_{k=0} = \sum_i |i\rangle \langle i| \otimes g^+(\omega)$. Here $g^+(\omega)$ is the 2×2 response matrix for a single noninteracting node, which manifests as a rotation matrix of a complex angle α_ω,

$$g^+(\omega) = \frac{1}{k_{0,\omega}}(I \cos\alpha_\omega - A_1 \sin\alpha_\omega), \quad \text{(C2)}$$

$$k_{0,\omega} = \sqrt{(k_g + i\omega\gamma - m\omega^2)^2 - (\omega\hat{B})^2}, \quad \text{(C3)}$$

$$\cos\alpha_\omega = \frac{1}{k_{0,\omega}}(k_g + i\omega\gamma - m\omega^2), \quad \text{(C4)}$$

$$\sin\alpha_\omega = \frac{1}{k_{0,\omega}} i\omega\hat{B}. \quad \text{(C5)}$$

The interacting part K consists of blocks

$$(-K)_{ii} = \langle i|(-K)|i \rangle = \sum_{j, j \neq i} \big(-e_{ij} e_{ij}^T \big), \quad \text{(C6)}$$

$$(-K)_{ji} = \langle j|(-K)|i \rangle = e_{ij} e_{ij}^T, \quad \text{(C7)}$$

where e_{ij} denotes the unit vector that points from the equilibrium position of i to that of j.

We insert resolution of identity $I = \sum_i |i\rangle \langle i|$ into the expansion (C1). As an example,

$$\langle i|G^+|_{k=0}(-K)G^+|_{k=0}(-K)G^+|_{k=0}|j \rangle$$
$$= \sum_m g^+(\omega)(-K)_{im} g^+(\omega)(-K)_{mj} g^+(\omega). \quad \text{(C8)}$$

For block $(-K)_{im}$ to be nonzero, either site i and site m are bonded, or $m = i$. Likewise for block $(-K)_{mj}$. These constraints on path $i \to m \to j$ can be conveniently addressed using diagrams: first draw the network, label the nodes i and j, then identify node m's that satisfy the constraints.

Now we apply the diagrammatic approach to energy flux for site i, Eq. (15) or Eq. (B34). Each term in the expansion of the energy flux can be represented as a diagram, or a path l: $i = l_0 \to l_1 \to \cdots \to l_{|l|-1} \to l_{|l|} = i$, where $|l|$ is the length of the path. Consecutive nodes in the path either have to be bonded or they are the same node. The path has to start and end at node i because of the existence of the projection operator P_i. The three G^+'s dictate that path l needs to be partitioned into three segments with lengths $\{|l|_1, |l|_2, |l|_3\}$ ($|l|_1 + |l|_2 + |l|_3 = |l|$), and each segment sets how each G^+ is expanded.

Taken together, the diagrammatic expression of $\langle Q_i^{(2)} \rangle_{B_t}$ can be written as a sum over paths,

$$\langle Q_i^{(2)} \rangle_{B_t} = T_a \sum_{n=1}^{\infty} T |\Delta \tilde{B}_n|^2 \sum_l k^{|l|} f_{i,n;l}, \quad \text{(C9)}$$

$$f_{i,n;l} = \sum_{|l|_1 + |l|_2 + |l|_3 = |l|} f_{i,n;l;|l|_1, |l|_2, |l|_3}. \quad \text{(C10)}$$

$f_{i,n;l}$ denotes the mathematical expression for path l. $f_{i,n;l;|l|_1, |l|_2, |l|_3}$ denotes the expression for partition $\{|l|_1, |l|_2, |l|_3\}$, which reads

$$f_{i,n;l;|l|_1, |l|_2, |l|_3}$$
$$= 2\,\text{Re} \int \frac{d\omega}{2\pi} \omega(\omega + \omega_n)(h(\omega + \omega_n)$$
$$- h(\omega)) \text{tr}\, \{M[(-K)g^+(\omega)]_{l_{|l|_1 + |l|_2} \to \cdots i} A$$
$$\times M[g^+(\omega + \omega_n)(-K)]_{l_{|l|_1} \to \cdots l_{|l|_1 + |l|_2}} g^+(\omega + \omega_n) A$$
$$\times M[g^+(-\omega)^T(-K)]_{i \to \cdots l_{|l|_1}} [g^+(-\omega)^T - g^+(\omega)] \}. \quad \text{(C11)}$$

Symbol $M[\cdot]$ denotes the expression for a segment of the path,

$$
M[(-K)g^+(\omega)]_{l_0 \to l_1 \to \cdots \to l_n}
$$
$$
= (-K)_{l_n,l_{n-1}} g^+(\omega) \cdots (-K)_{l_2,l_1} g^+(\omega)(-K)_{l_1,l_0} g^+(\omega),
$$
(C12)

$$
M[g^+(\omega)(-K)]_{l_0 \to l_1 \to \cdots \to l_n}
$$
$$
= g^+(\omega)(-K)_{l_n,l_{n-1}} \cdots g^+(\omega)(-K)_{l_2,l_1} g^+(\omega)(-K)_{l_1,l_0}.
$$
(C13)

From Eqs. (C9), (C10), and (C11), we obtain the procedure to write down energy flux for site i on the order of $k^{|l|}$ as follows. First, draw all possible closed paths with length $|l|$ that starts from node i, iteratively navigates to its bonded neighbors or to itself for $|l|$ steps, and ends at node i. Secondly, for each path l, find all partitions $\{|l|_1, |l|_2, |l|_3\}$ and calculate $f_{i,n;l;|l|_1,|l|_2,|l|_3}$ according to Eq. (C11). Finally, sum

up all partitions to get $f_{i,n;l}$ [Eq. (C10)], then sum up all paths to obtain $\langle Q_i^{(2)} \rangle$ on the $k^{|l|}$ order [Eq. (C9)].

Path l and its corresponding mathematical expression $f_{i,n;l}$ can be presented as diagrams. An arrow $i \to j$ in the diagram corresponds to $(-K)_{ji}$ mathematically and, as a result, if $i \neq j$, the contribution from this arrow is independent of the other neighbors of i or j [Eq. (C7)]. If $i = j$, however, neighbors of i cannot be removed because they do affect the value of $i \to i$ through $(-K)_{ii}$ [Eq. (C6)]. As a result, if a diagram contains no loops on some node j, the diagram is equal to a trimmed diagram where we remove all neighbors of j except for those appearing in the path. This basic property helps to simplify the diagrams without explicit calculations of $f_{i,n;l}$.

2. Diagrams that consist of only loops vanish

For diagrams with only loops, the expression $M[\cdot]$ simplifies to multiplication of the same matrix. Denoting $(-K)_{ii} = M_i$, $f_{i,n;l;|l|_1,|l|_2,|l|_3}$ reads

$$
f_{i,n;l;|l|_1,|l|_2,|l|_3} = f_{M_i,1}(|l|_1, |l|_2, |l|_3) - f_{M_i,2}(|l|_1, |l|_2, |l|_3),
$$
(C14)

$$
f_{M_i,1}(|l|_1, |l|_2, |l|_3) = 2\,\text{Re} \int \frac{d\omega}{2\pi} \omega(\omega + \omega_n)(h(\omega + \omega_n) - h(\omega))\,\text{tr}\,\{[M_i g^+(\omega)]^{|l|_3} A[g^+(\omega + \omega_n)M_i]^{|l|_2}
$$
$$
\times\, g^+(\omega + \omega_n)A[g^+(-\omega)^T M_i]^{|l|_1} g^+(-\omega)^T\},
$$
(C15)

$$
f_{M_i,2}(|l|_1, |l|_2, |l|_3) = 2\,\text{Re} \int \frac{d\omega}{2\pi} \omega(\omega + \omega_n)(h(\omega + \omega_n) - h(\omega))\,\text{tr}\,\{[M_i g^+(\omega)]^{|l|_3} A[g^+(\omega + \omega_n)M_i]^{|l|_2}
$$
$$
\times\, g^+(\omega + \omega_n)A[g^+(-\omega)^T M_i]^{|l|_1} g^+(\omega)\}.
$$
(C16)

From the above definitions, it is straightforward to prove the following three relations:

$$
f_{M_i,1}(|l|_1, |l|_2, |l|_3) = f_{M_i,2}(|l|_1 + 1, |l|_2, |l|_3 - 1),
$$
(C17)

$$
f_{M_i,1}(|l|_1, |l|_2, 0) = -f_{M_i,1}(|l|_2, |l|_1, 0),
$$
(C18)

$$
f_{M_i,2}(0, |l|_2, |l|_3) = -f_{M_i,2}(0, |l|_3, |l|_2).
$$
(C19)

With these relations, $f_{i,n;l}$ can be shown to be zero,

$$
f_{i,n;l} = \sum_{|l|_1+|l|_2+|l|_3=l} \{f_{M_i,1}(|l|_1, |l|_2, |l|_3)
$$
$$
- f_{M_i,2}(|l|_1, |l|_2, |l|_3)\}
$$
(C20)

$$
= \sum_{|l|_1=0}^{l-1} \sum_{|l|_2=0}^{l-1-|l|_1} f_{M_i,1}(|l|_1, |l|_2, l - |l|_1 - |l|_2)
$$

$$
+ \sum_{|l|_1=0}^{l} f_{M_i,1}(|l|_1, l - |l|_1, 0)
$$

$$
- \sum_{|l|_2=0}^{l} f_{M_i,2}(0, |l|_2, l - |l|_2)
$$

$$
- \sum_{|l|_1=1}^{l} \sum_{|l|_2=0}^{l-|l|_1} f_{M_i,2}(|l|_1, |l|_2, l - |l|_1 - |l|_2)
$$

$$
= 0.
$$
(C21)

Thus diagrams consisting of only loops vanish.

APPENDIX D: FLUX SCALING IN STAR-SHAPED NETWORKS

For a star-shaped network with evenly spaced branches, we numerically showed in Fig. 7(a) that the flux amplitude of the central node, $|Q_c|$, increases with the number of branches, N. In this section, we explain this observation using perturbation theory, and show that, in the perturbative regime, $|Q_c| \propto N^2$. We will analyze the flux on a side node, Q_s; then due to symmetry and energy balance, $Q_c = -NQ_s$.

Numerical calculations of fluxes at various values of $\Delta\hat{B}$ and k show that [Fig. 8(a)], as k decreases, the relation between Q_s and N approaches a linear relation.

Using our diagrammatic theory, the flux through side node 2 can be decomposed as the sum of three diagrams [Fig. 8(b)]. Diagrams $2 \to 2 \to 1 \to 2$ and $2 \to 1 \to 2 \to 2$ can be shown to vanish. Only diagram $2 \to 1 \to 1 \to 2$ survives.

The vanishing of diagrams 8(b1) and 8(b2) can be seen from their equivalent diagrams on a two-node network. Since there are no loops on node 1, all neighbors except for node 2 can be removed according to diagram property Fig. 3(a). For a two-node network, all fluxes vanish for symmetry reasons; so does the sum of all diagrams on the order of k^3,

$$
f_{2,n;2\to2\to1\to2}^{\text{2-node}} + f_{2,n;2\to1\to2\to2}^{\text{2-node}} + f_{2,n;2\to1\to1\to2}^{\text{2-node}} = 0. \quad \text{(D1)}
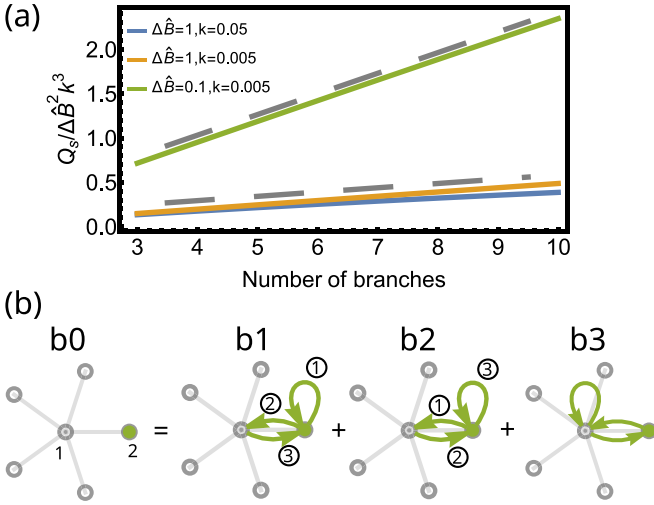$$

FIG. 8. (a) At small k's ($k = 0.005$ in the plot), the flux on a side node of star-shaped networks scales linearly with the number of side nodes. (b) Diagrammatic decomposition for flux through side node 2 of a star-shaped network with five branches. The modulation is a step function where $\hat{B}(t)$ switches between $-\Delta\hat{B}$ and $\Delta\hat{B}$. The period is taken to be infinite. All parameters except for $\Delta\hat{B}$ and k are set to 1.

$f_{i,n;l}$ denotes the flux for node i from B-field mode n and path l. The expression of $f_{i,n;l}$ itself is lengthy [Eqs. (C10) and (C11)], but comparisons between different paths can be simplified. The important components are blocks of the force matrix K [Eqs. (C6) and (C7)]. $f_{i,n;l}^{\text{2-node}}$ for three paths reads

$$f_{2,n;2\rightarrow2\rightarrow1\rightarrow2}^{\text{2-node}} = \sum \text{tr} \cdots (-K)_{21} \cdots (-K)_{12} \cdots (-K)_{22} \cdots ,$$
$$\text{(D2)}$$

$$f_{2,n;2\rightarrow1\rightarrow2\rightarrow2}^{\text{2-node}} = \sum \text{tr} \cdots (-K)_{22} \cdots (-K)_{21} \cdots (-K)_{12} \cdots ,$$
$$\text{(D3)}$$

$$f_{2,n;2\rightarrow1\rightarrow1\rightarrow2}^{\text{2-node}} = \sum \text{tr} \cdots (-K)_{21} \cdots (-K)_{11} \cdots (-K)_{12} \cdots ,$$
$$\text{(D4)}$$

where omitted parts $(\cdots)$ are identical for the three $f_{2,n;l}^{\text{2-node}}$'s. Plugging in the relation

$$(-K)_{11} = (-K)_{22} = -(-K)_{12} = -(-K)_{21} \qquad \text{(D5)}$$

for two-node networks, we see that the three $f_{2,n;l}^{\text{2-node}}$'s are equal. Since their sum is zero [Eq. (D1)], each of the three $f_{2,n;l}^{\text{2-node}}$'s equals zero and thus diagrams $2 \rightarrow 2 \rightarrow 1 \rightarrow 2$ and $2 \rightarrow 1 \rightarrow 2 \rightarrow 2$ vanish:

$$f_{2,n;2\rightarrow2\rightarrow1\rightarrow2}^{\text{2-node}} = f_{2,n;2\rightarrow1\rightarrow2\rightarrow2}^{\text{2-node}} = f_{2,n;2\rightarrow1\rightarrow1\rightarrow2}^{\text{2-node}} = 0. \quad \text{(D6)}$$

Due to equivalence of diagrams, corresponding diagrams for star-shaped networks vanish:

$$f_{2,n;2\rightarrow2\rightarrow1\rightarrow2}^{\text{star}} = f_{2,n;2\rightarrow1\rightarrow2\rightarrow2}^{\text{star}} = 0. \qquad \text{(D7)}$$

Now we analyze diagram $2 \rightarrow 1 \rightarrow 1 \rightarrow 2$. The formula for $f_{2,n;2\rightarrow2\rightarrow1\rightarrow2}^{\text{star}}$ has the same form as Eq. (D4), except that $(-K)_{11}$ becomes

$$(-K)_{11} = \sum_{j=2}^{N+1} \begin{pmatrix} \cos^2\theta_j & \cos\theta_j\sin\theta_j \\ \cos\theta_j\sin\theta_j & \sin^2\theta_j \end{pmatrix} = \frac{N}{2}\begin{pmatrix} 1 & 0 \\ 0 & 1 \end{pmatrix},$$
$$\text{(D8)}$$

where $\theta_j = 2\pi(j-2)/N + \phi$ is the orientation of the bond $1 - j$ and ϕ is an arbitrary phase. The second equality holds for $N \geqslant 3$.

As a result, the diagram $2 \rightarrow 1 \rightarrow 1 \rightarrow 2$ and thus the flux through a side node Q_s is proportional to the number of branches N. The flux through the central node $Q_c \propto N^2$.

[1] S. Flach, Y. Zolotaryuk, A. E. Miroshnichenko, and M. V. Fistul, Broken Symmetries and Directed Collective Energy Transport in Spatially Extended Systems, Phys. Rev. Lett. **88**, 184101 (2002).

[2] S. Das, O. Narayan, and S. Ramaswamy, Ratchet for energy transport between identical reservoirs, Phys. Rev. E **66**, 050103(R) (2002).

[3] N. Li, P. Hänggi, and B. Li, Ratcheting heat flux against a thermal bias, Europhys. Lett. **84**, 40009 (2008).

[4] J. Ren and B. Li, Emergence and control of heat current from strict zero thermal bias, Phys. Rev. E **81**, 021111 (2010).

[5] J. Ren, S. Liu, and B. Li, Geometric Heat Flux for Classical Thermal Transport in Interacting Open Systems, Phys. Rev. Lett. **108**, 210603 (2012).

[6] N. Li, J. Ren, L. Wang, G. Zhang, P. Hänggi, and B. Li, Colloquium: Phononics: Manipulating heat flow with electronic analogs and beyond, Rev. Mod. Phys. **84**, 1045 (2012).

[7] B. Sabass, Fluctuating, Lorentz-force-like coupling of Langevin equations and heat flux rectification, Phys. Rev. E **96**, 022109 (2017).

[8] K. Kanazawa, T. Sagawa, and H. Hayakawa, Heat conduction induced by non-Gaussian athermal fluctuations, Phys. Rev. E **87**, 052124 (2013).

[9] M. M. Cândido, W. A. M. Morgado, and S. M. Duarte Queirós, Macroscopic violation of the law of heat conduction, Phys. Rev. E **96**, 032143 (2017).

[10] E. H. Colombo, L. A. C. A. Defaveri, and C. Anteneodo, Heat flux direction controlled by power-law oscillators under non-Gaussian fluctuations, Phys. Rev. E **100**, 032118 (2019).

[11] L. Zhu and S. Fan, Persistent Directional Current at Equilibrium in Nonreciprocal Many-Body Near Field Electromagnetic Heat Transfer, Phys. Rev. Lett. **117**, 134303 (2016).

[12] L. Zhu, Y. Guo, and S. Fan, Theory of many-body radiative heat transfer without the constraint of reciprocity, Phys. Rev. B **97**, 094302 (2018).

[13] Y. Dubi and M. Di Ventra, Colloquium: Heat flow and thermoelectricity in atomic and molecular junctions, Rev. Mod. Phys. **83**, 131 (2011).

[14] P. Reimann, Brownian motors: Noisy transport far from equilibrium, Phys. Rep. **361**, 57 (2002).

[15] M. H. Kolodrubetz, F. Nathan, S. Gazit, T. Morimoto, and J. E. Moore, Topological Floquet-Thouless Energy Pump, Phys. Rev. Lett. **120**, 150601 (2018).

[16] Z. Liao, W. T. M. Irvine, and S. Vaikuntanathan, Rectification in Nonequilibrium Parity Violating Metamaterials, Phys. Rev. X **10**, 021036 (2020).

[17] L. M. Nash, D. Kleckner, A. Read, V. Vitelli, A. M. Turner, and W. T. M. Irvine, Topological mechanics of gyroscopic metamaterials, Proc. Natl. Acad. Sci. USA **112**, 14495 (2015).

[18] N. P. Mitchell, L. M. Nash, D. Hexner, A. M. Turner, and W. T. M. Irvine, Amorphous topological insulators constructed from random point sets, Nat. Phys. **14**, 380 (2018).

[19] P. Hanggi and P. Jung, Colored noise in dynamical systems, in *Advances in Chemical Physics* (John Wiley & Sons, New York, 1994), pp. 239–326.

[20] P. C. Martin, E. D. Siggia, and H. A. Rose, Statistical dynamics of classical systems, Phys. Rev. A **8**, 423 (1973).

[21] H.-K. Janssen, On a Lagrangean for classical field dynamics and renormalization group calculations of dynamical critical properties, Z. Physik B **23**, 377 (1976).

[22] C. De Dominicis and L. Peliti, Field-theory renormalization and critical dynamics above T_c: Helium, antiferromagnets, and liquid-gas systems, Phys. Rev. B **18**, 353 (1978).

[23] K. Sekimoto, Kinetic characterization of heat bath and the energetics of thermal ratchet models, J. Phys. Soc. Jpn. **66**, 1234 (1997).

[24] K. Sekimoto, Langevin equation and thermodynamics, Prog. Theor. Phys. Suppl. **130**, 17 (1998).

[25] C. Gardiner, The Ito calculus and stochastic differential equations, in *Stochastic Methods*, 4th ed. (Springer-Verlag, Berlin, Heidelberg, 2009), Chap. 4, p. 107.

[26] M. Ceriotti, G. Bussi, and M. Parrinello, Colored-noise thermostats à la carte, J. Chem. Theory Comput. **6**, 1170 (2010).

[27] P. Pradhan and U. Seifert, Nonexistence of classical diamagnetism and nonequilibrium fluctuation theorems for charged particles on a curved surface, Europhys. Lett. **89**, 37001 (2010).

[28] J. A. Hertz, Y. Roudi, and P. Sollich, Path integral methods for the dynamics of stochastic and disordered systems, J. Phys. A: Math. Theor. **50**, 033001 (2016).

[29] G. C. Wick, The Evaluation of the Collision Matrix, Phys. Rev. **80**, 268 (1950).

[30] A. Kundu, S. Sabhapandit, and A. Dhar, Large deviations of heat flow in harmonic chains, J. Stat. Mech. (2011) P03007.